Hanapi et al. *EPJ Quantum Technology* (2024) 11:51
https://doi.org/10.1140/epjqt/s40507-024-00263-9

EPJ Quantum Technology
a SpringerOpen Journal

RESEARCH Open Access

Nonclassical light in a three-waveguide coupler with second-order nonlinearity

Mohd Syafiq M. Hanapi[1], Abdel-Baset M. A. Ibrahim[1*], Rafael Julius[2], Pankaj K. Choudhury[3] and Hichem Eleuch[4,5]

*Correspondence:
abdelbaset@uitm.edu.my;
abdelbaset.ibrahim@gmail.com
[1]Faculty of Applied Sciences, Universiti Teknologi MARA (UiTM), 40450 Shah Alam, Selangor, Malaysia
Full list of author information is available at the end of the article

Abstract

Possible squeezed states generated in a three-waveguide nonlinear coupler operating with second harmonic generation is discussed. This study is carried out using two well-known techniques; the phase space method (based on positive-P representation) and the Heisenberg-based analytical perturbative (AP) method. The effects of key design parameters were investigated under various conditions, including full frequency matching, symmetrical and asymmetrical waveguide initialization, and both codirectional and contr-adirectional propagation. The system consistently produced long-lasting oscillatory squeezed states across all three waveguides, even when only one waveguide was pumped with coherent light while the others were in a vacuum state. Also, the performance and capacities of both methods are critically evaluated. For low levels of key design parameters and in the early stages of evolution, a high level of agreement between the two methods is noticed. In the new era of quantum-based technology, the proposed system opens a new avenue for utilising nonlinear couplers in nonclassical light generation.

Keywords: Quantum Optics; Second-Harmonic Generation; Nonlinear Coupler; Squeezed states

1 Introduction

Squeezed light is a Nonclassical light that is typically produced from the coherent state or vacuum state (of light) by specific optical nonlinear interactions, and it displays reduced noise in one of the two electric field quadrature components. Squeezed states of light have such unique noise distribution where at least one field quadrature falls below the shot noise level [1]. The need to search for efficient squeezed light sources is driven by their profound implications in enhancing measurement precision [2], advancing quantum communication [3], and enabling new applications in quantum information processing [4]. In particular, by facilitating precise quantum gate operations and reducing errors which are essential for reliable quantum computations [5]. Efficient squeezed light sources can significantly reduce quantum noise, thereby improving the sensitivity and accuracy of measurements in experiments and technologies operating at the quantum limit. This is particularly critical for gravitational wave detection [6], where detecting extremely weak signals

requires a substantial reduction in noise. In quantum communication, efficient squeezed light sources enhance the security and efficiency of quantum key distribution protocols by reducing noise and increasing the signal-to-noise ratio, enabling secure communication over long distances [7]. In medical imaging, squeezed light can enhance the resolution and contrast of imaging techniques [8, 9], leading to better visualization of biological tissues and structures [10, 11], which is essential for accurate diagnosis and treatment. Finally, the ability to produce squeezed light efficiently is essential for integrating these sources into compact and scalable photonic devices [12], which are key to the development of advanced quantum photonic circuits and optical communication systems. Therefore, the search for efficient squeezed light sources is a practical necessity for the advancement of various cutting-edge technologies.

Creating squeezed light requires nonlinear interactions, which can be achieved using various devices [13–16]. Although a single nonlinear waveguide can generate squeezed light, multi-waveguide devices provide several advantages over single-waveguide structures. They allow for more complex designs where coupling coefficients and waveguide separations can be finely tuned, providing greater control over squeezing parameters. By adjusting the relative phases and intensities in different waveguides, better phase-matching conditions can be achieved [17]. Additionally, multi-waveguide structures enhance nonlinear interactions [18]; optimizing these interactions across multiple waveguides results in higher degrees of squeezing compared to single waveguides. Multi-waveguide systems also improve the control of spatial modes, reducing noise [19] and enhancing the purity of squeezed states. Furthermore, multi-waveguide devices can perform complex operations such as beam splitting, multiplexing, and demultiplexing, which are not possible with single waveguides. These systems are more adaptable to integration with other photonic components on a single chip [20], leading to more scalable and compact designs for quantum photonic circuits.

To harness the benefits of multi-waveguide structures in generating nonclassical light, the nonlinear coupler (NLC) has been proposed [21–23]. An NLC consists of two closely spaced waveguides, each supporting one or more optical modes from a laser source. These waveguides exchange energy through the coupling of their evanescent fields. Quantum nonlinear optical couplers are simple and experimentally realizable. These integrate well with quantum optical devices, such as quantum circuits, photonic chips, and all-optical logic gates [24, 25]. In addition, the waveguide interaction length and coupling in the nonlinear coupler can also be used to regulate quantum phenomena. We may classify NLC into two distinct classes based on the number of waveguides: first, the typical two-waveguide devices that have been extensively investigated [26–29], and second, the recently suggested multi-waveguide class of devices [30–34]. The two-waveguide class of nonlinear couplers (NLCs) fundamentally exhibits nonclassical behavior. However, recently proposed multichannel NLCs could serve as superior sources of nonclassical light due to their rich design parameters and the additional advantages mentioned in the previous paragraph. The source of nonlinearity in NLCs can be the second [35] or third-order [36], or even a combination of both the linear and nonlinear [37]. Third-order nonlinear materials can set off a wide range of nonclassical effects. Yet, it is the second-order nonlinear medium that has a greater impact. Therefore, we believe that a multi-waveguide NLC operating with second-order nonlinearity should be a good nonclassical light generator.

To investigate the nonclassical features of light in our system, we employ two methods, rather than relying on a single theoretical prediction. This dual approach not only ensures accurate findings but also provides insights into the strengths and weaknesses of each method used. In previous research on quantum NLCs, the behavior of quantum systems is often exclusively explored with one of these methods. The first method is the phase space approach, a key technique under the Schrödinger picture. Here, the operators remain fixed while the state vector changes with time. By substituting the correct Hamiltonian for the system into the von Neumann equation of motion, we construct the master equation of the density matrix. We then employ positive-P representation to convert the dynamical master equation into its corresponding classical Fokker-Planck (FP) equation in the phase space [38, 39]. Using Ito rules, the FP equation is converted to an equivalent set of stochastic differential equations describing the evolution of the phase space variables. The positive-P method emphasizes accurate estimation by incorporating stochastic trajectories and the evolution of quantum systems is simulated without truncation [30–34]. The second method is the analytical perturbative (AP) approach based on the Heisenberg picture, where the field operators change over time while the state vector remains static. The AP method, initially introduced by Sen and Mandal [40] and later adopted by other researchers (see, e.g., [41, 42]), is an enhancement to the well-known short-length (or short-time) approximation method used by Perina and others to study various quantum systems (see, e.g., [43–45]). In the AP method, quantum-coupled nonlinear differential equations are obtained using the Heisenberg equation of motion. The solution of these coupled equations of motion is assumed in the form of the Baker–Campbell–Hausdorff (BCH) formula. The BCH formula is then expanded in terms of nested commutators truncated up to the second order to make the calculations manageable, assuming that higher-order commutators decrease in magnitude sufficiently fast, justifying their omission [40]. This is often valid in weak perturbation regimes but might not hold in strongly interacting systems. Consequently, the AP method is approximated because it relies on the truncated BCH formula. The mathematical description of the current three-waveguide system using both methods is detailed in the next section.

In our recent work [46], we demonstrated that a three-waveguide codirectional coupler system operating under frequency mismatching conditions might serve as a better alternative to the typical two-channel NLC or those operating with third-order Kerr nonlinearity. In this study, we employ both the AP and the phase space methods to examine the single-mode squeezing in three-channel NLC waveguides with second-order nonlinearity under both codirectional and contra-directional propagation. A single fundamental mode travels across each waveguide with fundamental frequency ω assuming full frequency matching. The fundamental photons of the pump field also generate second harmonic (SH) modes propagating along the fiber with double frequency (2ω). Figure 1 depicts a schematic illustration of the system under consideration for the case of codirectional (Fig. 1a) and contra-directional propagation (Fig. 1b). In codirectional propagation, all three modes $\hat{E}_1$, $\hat{E}_2$, and $\hat{E}_3$ propagate in the same direction, whereas in contra-directional propagation, one mode (Mode $\hat{E}_2$) is assumed to propagate in opposite direction. The effect of key design parameters on the generated squeezed states is examined under full frequency matching and for both codirectional and contra-directional propagation. Also, the performance and capacities of both methods are critically evaluated. The current triple-waveguide structure may provide a more efficient mechanism for generating nonclassical effects with en-

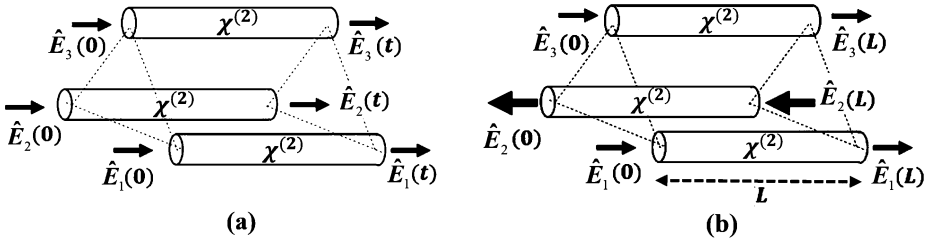

Figure 1 Basic diagram of the three-channel nonlinear coupler with second-order nonlinearity (a) codirectional propagation of three fundamental modes ($\hat{E}_1$, $\hat{E}_2$ and $\hat{E}_3$). (b) A contra-directional system where the mode $\hat{E}_2$ propagates opposite to the other two modes

hanced performance. This is because its coupled-mode interactions and correlations are more adaptable.

2 Mathematical formulation

Here, we describe the mathematical formulation of the system under consideration using both methods. We first construct the Hamiltonian which properly describes the system under consideration. For three-channel NLC devices, such Hamiltonian can be constructed as follows:

$$\begin{aligned}\hat{H} &= \hat{H}_{free} + \hat{H}_{Linear} + \hat{H}_{Nonlinear} + \hat{H}_{SHG} \\ &= \hbar\left[\omega_1\hat{a}_1^\dagger\hat{a}_1 + \omega_2\hat{a}_2^\dagger\hat{a}_2 + \omega_3\hat{a}_3^\dagger\hat{a}_3\right] + \hbar\kappa\left[\hat{a}_1^\dagger\hat{a}_2 + \hat{a}_2^\dagger\hat{a}_3 + \hat{a}_3^\dagger\hat{a}_1 + \text{h.c.}\right] \\ &+ \frac{ig}{2}\hbar\left[\left(\hat{a}_1^{\dagger 2}\hat{b}_1 + \hat{a}_2^{\dagger 2}\hat{b}_2 + \hat{a}_3^{\dagger 2}\hat{b}_3 - \text{h.c.}\right)\right] + \hbar\left[(2\omega_1)\,\hat{b}_1^\dagger\hat{b}_1 + (2\omega_2)\,\hat{b}_2^\dagger\hat{b}_2 + (2\omega_3)\,\hat{b}_3^\dagger\hat{b}_3\right]\end{aligned} \tag{1}$$

The free Hamiltonian $\hat{H}_{free}$ represents the three fundamental modes propagating in their channels with fundamental frequencies ω_1, ω_2, and ω_3, respectively. The Hamiltonian linear coupling $\hat{H}_{Linear}$ represents the linear coupling between each one of the three modes and the strength of the coupling is quantified by the linear coupling coefficient κ while h.c. stands for the Hermitian conjugate. This coupling is due to the overlapping of the evanescent waves of each propagating field mode. The $\hat{H}_{Nonlinear}$ represents the second-order nonlinear interaction between each fundamental mode and the relevant waveguide, and the strength of coupling is quantified by the nonlinear coupling coefficient g. Finally, the Hamiltonian $\hat{H}_{SHG}$ determines three SH modes propagating with frequencies $2\omega_1$, $2\omega_2$, and $2\omega_3$, respectively. The second-order nonlinear interaction process generates these modes with frequencies double those of the fundamental modes.

2.1 The phase-space method

To describe the dynamics of the density matrix evolution, the phase space method substitutes the full Hamiltonian into the von Neumann equation of motion. Following that, one of the representations might be used to transform the master equation to its classical Fokker-Planck (FP) equation in phase space. In this work, we use the positive-P representation. An initial time-dependent distribution function P is guaranteed to exist, to be positive, and to fulfill an FP equation in the positive-P representation. One method for solving the FP equation is to use Ito rules to determine the equivalent set of noisy coupled

stochastic equations. The phase space variables utilized to compute the required nonclassical states can be obtained by numerically solving these stochastic equations. We recall the standard form of the Liouville-Von Neumann equation.

$$i\hbar\frac{\partial\hat{\rho}}{\partial t} = \left[\hat{H},\hat{\rho}\right] \tag{2}$$

Substituting the total Hamiltonian from Eq. (1) into Eq. (2) yields the reduced dynamical equation of the density operator as

$$\begin{aligned}
\frac{\partial\hat{\rho}}{\partial t} &= i\omega_1\left(\hat{\rho}\hat{a}_1^\dagger\hat{a}_1 - \hat{a}_1^\dagger\hat{a}_1\hat{\rho}\right) + i\omega_2\left(\hat{\rho}\hat{a}_2^\dagger\hat{a}_2 - \hat{a}_2^\dagger\hat{a}_2\hat{\rho}\right) + i\omega_3\left(\hat{\rho}\hat{a}_3^\dagger\hat{a}_3 - \hat{a}_3^\dagger\hat{a}_3\hat{\rho}\right)\\
&+ i\kappa\left(\hat{\rho}\hat{a}_1^\dagger\hat{a}_2 - \hat{a}_1^\dagger\hat{a}_2\hat{\rho}\right) + i\kappa\left(\hat{\rho}\hat{a}_1\hat{a}_2^\dagger - \hat{a}_1\hat{a}_2^\dagger\hat{\rho}\right) + i\kappa\left(\hat{\rho}\hat{a}_2^\dagger\hat{a}_3 - \hat{a}_2^\dagger\hat{a}_3\hat{\rho}\right)\\
&+ i\kappa\left(\hat{\rho}\hat{a}_2\hat{a}_3^\dagger - \hat{a}_2\hat{a}_3^\dagger\hat{\rho}\right) + i\kappa\left(\hat{\rho}\hat{a}_3^\dagger\hat{a}_1 - \hat{a}_3^\dagger\hat{a}_1\hat{\rho}\right) + i\kappa\left(\hat{\rho}\hat{a}_3\hat{a}_1^\dagger - \hat{a}_3\hat{a}_1^\dagger\hat{\rho}\right)\\
&+ \frac{g}{2}\left(\hat{a}_1^{\dagger 2}\hat{b}_1\hat{\rho} - \hat{\rho}\hat{a}_1^{\dagger 2}\hat{b}_1\right) + \frac{g}{2}\left(\hat{a}_2^{\dagger 2}\hat{b}_2\hat{\rho} - \hat{\rho}\hat{a}_2^{\dagger 2}\hat{b}_2\right) + \frac{g}{2}\left(\hat{a}_3^{\dagger 2}\hat{b}_3\hat{\rho} - \hat{\rho}\hat{a}_3^{\dagger 2}\hat{b}_3\right)\\
&+ \frac{g}{2}\left(\hat{\rho}\hat{a}_1^2\hat{b}_1^\dagger - \hat{a}_1^2\hat{b}_1^\dagger\hat{\rho}\right) + \frac{g}{2}\left(\hat{\rho}\hat{a}_2^2\hat{b}_2^\dagger - \hat{a}_2^2\hat{b}_2^\dagger\hat{\rho}\right) + \frac{g}{2}\left(\hat{\rho}\hat{a}_3^2\hat{b}_3^\dagger - \hat{a}_3^2\hat{b}_3^\dagger\hat{\rho}\right)\\
&+ i2\omega_1\left(\hat{\rho}\hat{b}_1^\dagger\hat{b}_1 - \hat{b}_1^\dagger\hat{b}_1\hat{\rho}\right) + i2\omega_2\left(\hat{\rho}\hat{b}_2^\dagger\hat{b}_2 - \hat{b}_2^\dagger\hat{b}_2\hat{\rho}\right) + i2\omega_3\left(\hat{\rho}\hat{b}_3^\dagger\hat{b}_3 - \hat{b}_3^\dagger\hat{b}_3\hat{\rho}\right)
\end{aligned} \tag{3}$$

Equation (3) is a quantum mechanical partial differential equation. It describes the time evolution of the density operator $\hat{\rho}$. However, this equation is difficult to solve. The standard method in quantum optics is to convert it to the corresponding classical c-number FP equation using one of the available representations such as positive-P or Wigner. Here we employ the positive-P representation with these quantum-classical operator correspondences [38, 39].

$$\hat{a}^\dagger\hat{\rho} = \left(\beta - \frac{\partial}{\partial\alpha}\right)P, \hat{a}\hat{\rho} = \alpha P, \hat{\rho}\hat{a} = \left(\alpha - \frac{\partial}{\partial\beta}\right)P, \hat{\rho}\hat{a}^\dagger = \beta P \tag{4}$$

The quantum-classical correspondences in positive-P representation map the evolution of the density matrix $\hat{\rho}$ to a classical probability distribution $P(\alpha,\beta,t)$ in phase space where α and β are independent complex variables. The FP equation may then be expressed as a collection of noisy stochastic equations obeying Ito principles, which is a standard approach in statistical mechanics [47]. For the present system, the following stochastic differential equations result from the process:

$$\frac{d\alpha_1}{dt} = -i\omega_1\alpha_1 + g\bar{\alpha}_1\beta_1 - i\kappa\alpha_2 - i\kappa\alpha_3 + \sqrt{g\bar{\alpha}_1}\eta_1(t) \tag{5}$$

$$\frac{d\bar{\alpha}_1}{dt} = -i(2\omega_1)\bar{\alpha}_1 - \frac{g}{2}\alpha_1^2 \tag{6}$$

$$\frac{d\beta_1}{dt} = i\omega_1\beta_1 + g\alpha_1\bar{\beta}_1 + i\kappa\beta_2 + i\kappa\beta_3 + \sqrt{g\bar{\beta}_1}\eta_2(t) \tag{7}$$

$$\frac{d\bar{\beta}_1}{dt} = i(2\omega_1)\bar{\beta}_1 - \frac{g}{2}\beta_1^2 \tag{8}$$

$$\frac{d\alpha_2}{dt} = -i\omega_2\alpha_2 + g\bar{\alpha}_2\beta_2 - i\kappa\alpha_1 - i\kappa\alpha_3 + \sqrt{g\bar{\alpha}_2}\eta_3(t) \tag{9}$$

$$\frac{d\bar{\alpha}_2}{dt} = -i\,(2\omega_2)\,\bar{\alpha}_2 - \frac{g}{2}\alpha_2^2 \tag{10}$$

$$\frac{d\beta_2}{dt} = i\omega_2\beta_2 + g\alpha_2\bar{\beta}_2 + i\kappa\beta_1 + i\kappa\beta_3 + \sqrt{g\bar{\beta}_2}\eta_4\,(t) \tag{11}$$

$$\frac{d\bar{\beta}_2}{dt} = i\,(2\omega_2)\,\bar{\beta}_2 - \frac{g}{2}\beta_2^2 \tag{12}$$

$$\frac{d\alpha_3}{dt} = -i\omega_3\alpha_3 + g\bar{\alpha}_3\beta_3 - i\kappa\alpha_2 - i\kappa\alpha_1 + \sqrt{g\bar{\alpha}_3}\eta_5\,(t) \tag{13}$$

$$\frac{d\bar{\alpha}_3}{dt} = -i\,(2\omega_3)\,\bar{\alpha}_3 - \frac{g}{2}\alpha_3^2 \tag{14}$$

$$\frac{d\beta_3}{dt} = i\omega_3\beta_3 + i\kappa\beta_2 + g\alpha_3\bar{\beta}_3 + i\kappa\beta_1 + \sqrt{g\bar{\beta}_3}\eta_6\,(t) \tag{15}$$

$$\frac{d\bar{\beta}_2}{dt} = i\,(2\omega_3)\,\bar{\beta}_2 - \frac{g}{2}\beta_3^2 \tag{16}$$

In Eqs. (5)–(16), we can simplify the picture by considering that α_i and β_i are the classical equivalence of the operators $\hat{a}_i$ and $\hat{a}_i^\dagger$ (i = 1, 2, and 3), respectively, while $\bar{\alpha}_i$ and $\bar{\beta}_i$ are the classical equivalent of the operators $\hat{b}_i$ and $\hat{b}_i^\dagger$. Therefore, for the three fundamental modes, we have three sets of variables (α_i, β_i) while for the three SH modes, we have another three sets of these classical complex variables $\left(\bar{\alpha}_i, \bar{\beta}_i\right)$. Note that, Eqs. (5)–(10) contain fluctuating forces $\eta_i\,(t)$ (i = 1, 2, 3, 4, 5 and 6). These fluctuations have zero mean and are correlated in time $\left\langle \eta_i\,(t)\,\eta_j\left(t'\right)\right\rangle = \delta_{ij}\delta\left(t - t'\right)$. As a result, the noise will dominate any single trajectory solution to these equations. A stable solution can only be obtained by averaging it across many trajectories.

2.2 The Analytical Perturbative (AP) method

The AP method has been used to study the quantum behaviour of a variety of systems [40–42]. This technique has time-efficient numerical computation since it requires a single operation only. In this approach, quantum-coupled nonlinear differential equations are obtained by plugging in the proper Hamiltonian or the momentum operator into the Heisenberg equation of motion. The solution of these coupled equations of motion is assumed in the form of the BCH formula, which is then expanded as a Taylor series up to the second order, and the intuitive analytical solution is proposed based on that expansion. As this technique is Schrödinger-picture based, the evolution of each operator is individually described through the quantum mechanical Heisenberg equation of motion, generally expressed as

$$i\hbar\frac{d\hat{a}_j}{dt} = \left[\hat{a}_j, \hat{H}\right] \tag{17}$$

Substituting the Hamiltonian from Eq. (1) into Eq. (17) for operators $\hat{a}_1$, $\hat{a}_2$, $\hat{a}_3$, $\hat{b}_1$, $\hat{b}_2$ and $\hat{b}_3$, we obtain the following coupled system of equations, which describes the time evolution of the operators, as follows:

$$\frac{d\hat{a}_1}{dt} = i\omega_1\hat{a}_1 + g\hat{a}_1^\dagger\hat{b}_1 + i\kappa\hat{a}_2 + i\kappa\hat{a}_3 \tag{18}$$

$$\frac{d\hat{a}_2}{dt} = i\omega_2\hat{a}_2 + g\hat{a}_2^\dagger\hat{b}_2 + i\kappa\hat{a}_1 + i\kappa\hat{a}_3 \tag{19}$$

$$\frac{d\hat{a}_3}{dt} = i\omega_3\hat{a}_3 + g\hat{a}_3^{\dagger}\hat{b}_3 + i\kappa\hat{a}_2 + i\kappa\hat{a}_1 \tag{20}$$

$$\frac{d\hat{b}_1}{dt} = i\,(2\omega_1)\,\hat{b}_1 - \frac{g}{2}\hat{a}_1^2 \tag{21}$$

$$\frac{d\hat{b}_2}{dt} = i\,(2\omega_2)\,\hat{b}_2 - \frac{g}{2}\hat{a}_2^2 \tag{22}$$

$$\frac{d\hat{b}_3}{dt} = i\,(2\omega_3)\,\hat{b}_3 - \frac{g}{2}\hat{a}_3^2 \tag{23}$$

Equations (18)–(20) in the previous set of coupled equations describe the propagation of operators representing the fundamental modes while Eqs. (21)–(23) describe the propagation of the operators representing the SH modes. Solutions to these equations are assumed to satisfy the Baker-Campbell-Hausdorff (BCH) formula, as follows.

$$\begin{aligned}\hat{a}_j = \exp\left(\frac{i}{\hbar}\hat{H}t\right)\hat{a}_j(0)\exp\left(-\frac{i}{\hbar}\hat{H}t\right) &= \hat{a}_j(0) + \frac{it}{\hbar}\left[\hat{H},\hat{a}_j(0)\right] \\ &- \frac{1}{2}\frac{t^2}{\hbar^2}\left[\hat{H},\left[\hat{H},\hat{a}_j(0)\right]\right] + \cdots\end{aligned} \tag{24}$$

For each operator ($\hat{a}_1$, $\hat{a}_2$, $\hat{a}_3$, $\hat{b}_1$, $\hat{b}_2$ and $\hat{b}_3$), the commutation relations $\left[\hat{H},\hat{a}_j(0)\right]$ and $\left[\hat{H},\left[\hat{H},\hat{a}_j(0)\right]\right]$ in Eq. (24) is evaluated utilizing Eqs. (18)–(23) to obtain the intuitive operator solutions of the following forms:

$$\begin{aligned}\hat{a}_1(t) = {} & \hat{a}_1(0)\,\mathrm{A}_1 + \hat{a}_2(0)\,\mathrm{A}_2 + \hat{a}_3(0)\,\mathrm{A}_3 + \hat{a}_1^{\dagger}(0)\,\hat{b}_1(0)\,\mathrm{A}_4 + \hat{a}_2^{\dagger}(0)\,\hat{b}_2(0)\,\mathrm{A}_5 \\ & + \hat{a}_3^{\dagger}(0)\,\hat{b}_3(0)\,\mathrm{A}_6 + \hat{a}_2^{\dagger}(0)\,\hat{b}_1(0)\,\mathrm{A}_7 + \hat{a}_3^{\dagger}(0)\,\hat{b}_1(0)\,\mathrm{A}_8 + \mathrm{A}_9\,\hat{a}_1\hat{b}_1^{\dagger}\hat{b}_1 + \mathrm{A}_{10}\,\hat{a}_1^{\dagger}\hat{a}_1^2\end{aligned} \tag{25}$$

$$\begin{aligned}\hat{a}_2(t) = {} & \hat{a}_1(0)\,\mathrm{B}_1 + \hat{a}_2(0)\,\mathrm{B}_2 + \hat{a}_3(0)\,\mathrm{B}_3 + \hat{a}_1^{\dagger}(0)\,\hat{b}_2(0)\,\mathrm{B}_4 + \hat{a}_1^{\dagger}(0)\,\hat{b}_1(0)\,\mathrm{B}_5 \\ & + \hat{a}_2^{\dagger}(0)\,\hat{b}_2(0)\,\mathrm{B}_6 + \hat{a}_3^{\dagger}(0)\,\hat{b}_3(0)\,\mathrm{B}_7 + \hat{a}_3^{\dagger}(0)\,\hat{b}_2(0)\,\mathrm{B}_8 + \mathrm{B}_9\,\hat{a}_2\hat{b}_2^{\dagger}\hat{b}_2 + \mathrm{B}_{10}\,\hat{a}_2^{\dagger}\hat{a}_2^2\end{aligned} \tag{26}$$

$$\begin{aligned}\hat{a}_3(t) = {} & \hat{a}_1(0)\,\mathrm{C}_1 + \hat{a}_2(0)\,\mathrm{C}_2 + \hat{a}_3(0)\,\mathrm{C}_3 + \hat{a}_1^{\dagger}(0)\,\hat{b}_3(0)\,\mathrm{C}_4 + \hat{a}_2^{\dagger}(0)\,\hat{b}_2(0)\,\mathrm{C}_5 \\ & + \hat{a}_1^{\dagger}(0)\,\hat{b}_1(0)\,\mathrm{C}_6 + \hat{a}_3^{\dagger}(0)\,\hat{b}_3(0)\,\mathrm{C}_7 + \hat{a}_3(0)\,\hat{b}_3^{\dagger}(0)\,\hat{b}_3(0)\,\mathrm{C}_8 \\ & + \mathrm{C}_9\,\hat{a}_2^{\dagger}\hat{b}_3 + \mathrm{C}_{10}\,\hat{a}_3^{\dagger}\hat{a}_3^2\end{aligned} \tag{27}$$

$$\begin{aligned}\hat{b}_1(t) = {} & \mathrm{D}_1\,\hat{b}_1(0) + \mathrm{D}_2\,\hat{a}_1^2(0) + \mathrm{D}_3\,\hat{a}_2(0)\,\hat{a}_1(0) + \mathrm{D}_4\,\hat{a}_3(0)\,\hat{a}_1(0) \\ & + \mathrm{D}_5\,\hat{a}_1^{\dagger}(0)\,\hat{a}_1(0)\,\hat{b}_1(0) + \mathrm{D}_6\,\hat{a}_1(0)\,\hat{a}_1^{\dagger}(0)\,\hat{b}_1(0)\end{aligned} \tag{28}$$

$$\begin{aligned}\hat{b}_2(t) = {} & \mathrm{E}_1\,\hat{b}_2(0) + \mathrm{E}_2\,\hat{a}_2^2(0) + \mathrm{E}_3\,\hat{a}_1(0)\,\hat{a}_2(0) + \mathrm{E}_4\,\hat{a}_3(0)\,\hat{a}_2(0) \\ & + \mathrm{E}_5\,\hat{a}_2^{\dagger}(0)\,\hat{a}_2(0)\,\hat{b}_2(0) + \mathrm{E}_6\,\hat{a}_2(0)\,\hat{a}_2^{\dagger}(0)\,\hat{b}_2(0)\end{aligned} \tag{29}$$

$$\begin{aligned}\hat{b}_3(t) = {} & \mathrm{F}_1\,\hat{b}_3(0) + \mathrm{F}_2\,\hat{a}_2(0)\,\hat{a}_3(0) + \mathrm{F}_3\,\hat{a}_1(0)\,\hat{a}_3(0) + \mathrm{F}_4\,\hat{a}_3^2(0) \\ & + \mathrm{F}_5\,\hat{a}_3^{\dagger}(0)\,\hat{a}_3(0)\,\hat{b}_3(0) + \mathrm{F}_6\,\hat{a}_3(0)\,\hat{a}_3^{\dagger}(0)\,\hat{b}_3(0)\end{aligned} \tag{30}$$

In the analytical method, it is common to assume a weak nonlinear interaction in the form of a perturbation and ignore the higher-order nonlinear coupling terms. However, in the previous operator solutions in Eqs. (25)–(30), we have retained all nonlinear terms, i.e., both terms containing nonlinear coefficients g and those with g^2. The coefficients

$\{\boldsymbol{A}_k(t)\}_1^{10}$, $\{\boldsymbol{B}_k(t)\}_1^{10}$, $\{\boldsymbol{C}_k(t)\}_1^{10}$, $\{\boldsymbol{D}_k(t)\}_1^{6}$, $\{\boldsymbol{E}_k(t)\}_1^{6}$ and $\{\boldsymbol{F}_k(t)\}_1^{6}$ are all time-dependent. In the well-known short-length approximation method, these coefficients are essentially approximated by the second-degree polynomials in time. The AP method is superior to the short-length approximation method because these coefficients are evaluated precisely using additional mathematical steps. Basically, in the AP approach, sets of coupled differential equations describing these coefficients are derived by substituting the previous operator solutions in Eqs. (25)–(30) back into the operator evolution Eqs. (18)–(23) and equating similar terms on both sides. To obtain the coefficients, these sets of equations are numerically solved (please see Appendix A).

2.3 Calculation of single-mode squeezing

In quantum optics, the electric field operator for a single mode $\hat{E}_j(t)$ can be expressed in terms of two quadrature operators, X and Y, as $\hat{E}_j(t) = E_0\left(\hat{X}_j cos(\omega t) + \hat{Y}_j sin(\omega t)\right)$. The optical field quadrature operators are written in terms of creation and annihilation operators as $\hat{X}_j = \frac{1}{2}\left(\hat{a}_j + \hat{a}_j^\dagger\right)$ and $\hat{Y}_j = \frac{1}{2i}\left(\hat{a}_j - \hat{a}_j^\dagger\right)$ and $\left\langle(\Delta\hat{X}_j)^2\right\rangle$, $\left\langle(\Delta\hat{Y}_j)^2\right\rangle$ are their variances. For coherent light, the noise or uncertainty is equally distributed between these two quadratures. In squeezed states, however, the uncertainty in one quadrature component is reduced below the standard noise limit of a coherent state, while the uncertainty in the orthogonal quadrature is increased. This trade-off ensures that the Heisenberg uncertainty principle is not violated [1], i.e., $\left\langle(\Delta\hat{X}_j)^2\right\rangle < \frac{1}{4}$ or $\left\langle(\Delta\hat{Y}_j)^2\right\rangle < \frac{1}{4}$ where $\left\langle(\Delta\hat{X}_j)^2\right\rangle = \left\langle\hat{X}_j^2\right\rangle - \left\langle\hat{X}_j\right\rangle^2$ and $\left\langle(\Delta\hat{Y}_j)^2\right\rangle = \left\langle\hat{Y}_j^2\right\rangle - \left\langle\hat{Y}_j\right\rangle^2$. These quadrature variances are expressed in terms of the creation and annihilation operators as

$$\begin{bmatrix}\left\langle(\Delta\hat{X}_j)^2\right\rangle\\ \left\langle(\Delta\hat{Y}_j)^2\right\rangle\end{bmatrix} = \frac{1}{4}\left\{1 + 2\left\langle\hat{a}_j^\dagger\hat{a}_j\right\rangle - 2\left\langle\hat{a}_j^\dagger\right\rangle\left\langle\hat{a}_j\right\rangle \pm \left[\left\langle\hat{a}_j^2\right\rangle - \left\langle\hat{a}_j\right\rangle^2 + \left\langle\hat{a}_j^{\dagger 2}\right\rangle - \left\langle\hat{a}_j^\dagger\right\rangle^2\right]\right\} \tag{31}$$

$j = 1, 2, 3.$

In the preceding equation, j is the operator number and the bracket < > represents the normal-ordered expectation value, which necessitates the creation operators to be always to the left of the annihilation operators in any of their products. In the phase space method, the operators $\hat{a}_j$ and $\hat{a}_j^\dagger$ in Eq. (31) are replaced with their classical equivalence, i.e., the complex phase space variables α_j and β_j respectively. This yields the following equation of the quadrature variances of the field in phase space:

$$\begin{bmatrix}\left\langle(\Delta\hat{X}_j)^2\right\rangle\\ \left\langle(\Delta\hat{Y}_j)^2\right\rangle\end{bmatrix} = \frac{1}{4}\left\{1 + 2\left\langle\beta_j\alpha_j\right\rangle - 2\left\langle\beta_j\right\rangle\left\langle\alpha_j\right\rangle \pm \left[\left\langle\alpha_j^2\right\rangle - \left\langle\alpha_j\right\rangle^2 + \left\langle\beta_j^2\right\rangle - \left\langle\beta_j\right\rangle^2\right]\right\} \tag{32}$$

$j = 1, 2, 3.$

For the analytical method, expressions for the quadrature variances of the fundamental modes are obtained by substituting the operator solutions from Eqs. (25)–(27) into Eq. (31) and utilizing the classical equivalence $\left\langle\hat{a}_j(0)\right\rangle = \alpha_j$ and $\left\langle\hat{b}_j(0)\right\rangle = \beta_j$ results in the

field quadratures expressions shown below:

$$\begin{aligned}\begin{bmatrix}\left\langle\left(\Delta\hat{X}_1\right)^2\right\rangle\\ \left\langle\left(\Delta\hat{Y}_1\right)^2\right\rangle\end{bmatrix} &= 1/4\big[1+2\left(|\mathrm{A}_5|^2\,|\beta_2|^2+|\mathrm{A}_6|^2\,\beta_3^*\beta_3+\mathrm{A}_7\,\mathrm{A}_5^*\,\beta_2^*\beta_1\right.\\ &+\mathrm{A}_8\,\mathrm{A}_6^*\,\beta_3^*\beta_1+\mathrm{A}_5\,\mathrm{A}_7^*\,\beta_1^*\beta_2+\mathrm{A}_6\,\mathrm{A}_8^*\,\beta_1^*\beta_3\big)\\ &\pm\left(\mathrm{A}_4\,\mathrm{A}_1\,\beta_1+\mathrm{A}_{10}\,\mathrm{A}_1\,\alpha_1^2+\mathrm{A}_5\,\mathrm{A}_2\,\beta_2+\mathrm{A}_7\,\mathrm{A}_2\,\beta_1\right.\\ &+\mathrm{A}_6\,\mathrm{A}_3\,\beta_3+\mathrm{A}_8\,\mathrm{A}_3\,\beta_1+\mathrm{c}\,.c.\big)\big]\end{aligned} \tag{33}$$

$$\begin{aligned}\begin{bmatrix}\left\langle\left(\Delta\hat{X}_2\right)^2\right\rangle\\ \left\langle\left(\Delta\hat{Y}_2\right)^2\right\rangle\end{bmatrix} &= 1/4\big[1+2\left(|\mathrm{B}_5|^2\,|\beta_1|^2+|\mathrm{B}_7|^2\,|\beta_3|^2+\mathrm{B}_5\,\mathrm{B}_4^*\,\beta_2^*\beta_1\right.\\ &+\mathrm{B}_4\,\mathrm{B}_5^*\,\beta_1^*\beta_2+\mathrm{B}_8\,\mathrm{B}_7^*\,\beta_3^*\beta_2+\mathrm{B}_7\,\mathrm{B}_8^*\,\beta_2^*\beta_3\big)\\ &\pm\left(\mathrm{B}_4\,\mathrm{B}_1\,\beta_2+\mathrm{B}_5\,\mathrm{B}_1\,\beta_1+\mathrm{B}_6\,\mathrm{B}_2\,\beta_2+\mathrm{B}_{10}\,B_2\alpha_2^2\right.\\ &+\mathrm{B}_7\,\mathrm{B}_3\,\beta_3+\mathrm{B}_8\,\mathrm{B}_3\,\beta_2+\mathrm{c}\,.c.\big)\big]\end{aligned} \tag{34}$$

$$\begin{aligned}\begin{bmatrix}\left\langle\left(\Delta\hat{X}_3\right)^2\right\rangle\\ \left\langle\left(\Delta\hat{Y}_3\right)^2\right\rangle\end{bmatrix} &= 1/4\big[1+2\big(|\,\mathrm{C}_5\,|^2|\beta_2|^2+|\,\mathrm{C}_6\,|^2|\beta_1|^2+\mathrm{C}_6\,\mathrm{C}_4^*\,\beta_3^*\beta_1+\mathrm{C}_4\,\mathrm{C}_6^*\,\beta_1^*\beta_3\\ &+\mathrm{C}_5\,\mathrm{C}_9^*\,\beta_3^*\beta_2\big)\\ &\pm\left(\mathrm{C}_4\,\mathrm{C}_1\,\beta_3+\mathrm{C}_6\,\mathrm{C}_1\,\beta_1+\mathrm{C}_5\,\mathrm{C}_2\,\beta_2+\mathrm{C}_9\,\mathrm{C}_2\,\beta_3+\mathrm{C}_7\,\mathrm{C}_3\,\beta_3\right.\\ &+\mathrm{C}_{10}\,\mathrm{C}_3\,\alpha_3^2+\mathrm{c}\,.c.\big)\big]\end{aligned} \tag{35}$$

where c.c. symbolizes the complex conjugate. A brief schematic diagram summarizing the mathematical steps for both the phase space method and the analytical perturbative method is provided in Appendix B to clarify the previous mathematical procedures.

2.4 The contra-directional propagation

In codirectional propagation, all light modes travel in the same direction, as shown in Fig. 1a. This maximizes the interaction length between the waveguides, enhancing nonlinear interactions. Additionally, phase matching, mode coupling, dispersion management, and energy transfer between modes are more straightforward, making it easier to achieve improved squeezing within the waveguide coupler [48–50]. In contrast, contra-directional propagation, depicted in Fig. 1b, involves some modes propagating in the opposite direction. This setup can be used to control the degree of squeezing by varying the phase mismatch between the propagating modes due to back-reflection and phase reversal effects. However, the effective interaction length in contra-directional systems might be shorter due to the opposing travel directions, which can reduce the efficiency of nonlinear interactions. Despite this, novel interference effects can emerge, potentially enhancing certain squeezing characteristics. In addition, contra-directional systems can inherently provide some level of optical isolation, reducing noise from back-reflected signals. This isolation can help maintain the purity of the squeezed states, though it also makes phase matching more challenging. In terms of applications, codirectional propagation is advantageous

for long-distance quantum communication links where stable and high-quality squeezed states are required [51]. Contra-directional systems, on the other hand, might offer benefits in interferometric setups, where phase reversal and back-reflection can be used to enhance measurement sensitivity.

In the investigation of the contra-directional propagation, we follow the same procedure proposed by Perina [44, 45] and subsequently by others [52, 53]. First, the temporal system is converted into a spatial system. The conversion can be done using the time-displacement formula $dt = \frac{dz}{v_c}$, where v_c is the speed mode. Second, an opposite sign is introduced to the spatial equations of the contra-propagating mode $\hat{E}_2$ as shown in Fig. 1(b). In phase space method, the conversion is made to the stochastics differential Eqs. (5)–(16) by dividing both sides of each equation by v_c and introducing a negative sign to the spatial equations of the second mode $\hat{E}_2$. In this case, the Stochastic set of differential equations representing the contra-directional case can be written as

$$\frac{d\alpha_1}{dz} = -ik_1\alpha_1 + G\bar{\alpha}_1\beta_1 - iK\alpha_2 - iK\alpha_3 + \sqrt{G\bar{\alpha}_1}\xi_1(z) \tag{36}$$

$$\frac{d\beta_1}{dz} = ik_1\beta_1 + G\alpha_1\bar{\beta}_1 + iK\beta_2 + iK\beta_3 + \sqrt{G\bar{\beta}_1}\xi_2(t) \tag{37}$$

$$\frac{d\alpha_2}{dz} = +ik_2\alpha_2 - G\bar{\alpha}_2\beta_2 + iK\alpha_1 + iK\alpha_3 - \sqrt{G\bar{\alpha}_2}\xi_3(t) \tag{38}$$

$$\frac{d\beta_2}{dz} = -ik_2\beta_2 - G\alpha_2\bar{\beta}_2 - iK\beta_1 - iK\beta_3 - \sqrt{G\bar{\beta}_2}\xi_4(t) \tag{39}$$

$$\frac{d\alpha_3}{dz} = -ik_3\alpha_3 + G\bar{\alpha}_3\beta_3 - iK\alpha_2 - iK\alpha_1 + \sqrt{G\bar{\alpha}_3}\xi_5(t) \tag{40}$$

$$\frac{d\beta_3}{dz} = ik_3\beta_3 + iK\beta_2 + G\alpha_3\bar{\beta}_3 + iK\beta_1 + \sqrt{G\bar{\beta}_3}\xi_6(t) \tag{41}$$

$$\frac{d\bar{\alpha}_1}{dz} = -i(2k_1)\bar{\alpha}_1 - \frac{G}{2}\alpha_1^2 \tag{42}$$

$$\frac{d\bar{\beta}_1}{dz} = i(2k_1)\bar{\beta}_1 - \frac{G}{2}\beta_1^2 \tag{43}$$

$$\frac{d\bar{\alpha}_2}{dz} = -i(2k_2)\bar{\alpha}_2 - \frac{G}{2}\alpha_2^2 \tag{44}$$

$$\frac{d\bar{\beta}_2}{dz} = i(2k_2)\bar{\beta}_2 - \frac{G}{2}\beta_2^2 \tag{45}$$

$$\frac{d\bar{\alpha}_3}{dz} = -i(2k_3)\bar{\alpha}_3 - \frac{G}{2}\alpha_3^2 \tag{46}$$

$$\frac{d\bar{\beta}_2}{dz} = i(2k_3)\bar{\beta}_2 - \frac{G}{2}\beta_3^2 \tag{47}$$

In the previous system (36)–(47), we have used $k_j = \frac{\omega_j}{v_c}$, with j = 1,2,3, $G = \frac{g}{v_c}$, $K = \frac{\kappa}{v_c}$ and $\xi_l(z) = \frac{\eta_l(t)}{\sqrt{v_c}}$ with $l = 1, 2, \ldots, 6$. For the AP method, the same process is also performed on the set of equations (A1)-(A48). It is important to note that the Hamiltonian (1) describes the fields at all points of the interaction volume. This means that the spatial description is accurate only when the forward wave reaches $z = L$ and the backward wave reaches $z = 0$. However, it does not accurately describe the transient states of the contra-propagating fields for $0 < z < L$. For all operators in Eq. (1), this formulation guarantees the conservation of the boson commutation rules in both forward and backward propagating fields.

2.5 Numerical procedure

To summarize the numerical strategy for the phase space method, the system of Eqs. (5)–(16) is integrated numerically using the fourth-order Runge-Kutta method. As explained earlier, averaging across many trajectories is required to obtain a stable solution, which yields numerical values of (α_i, β_i) for the three fundamental modes and $(\bar{\alpha}_i, \bar{\beta}_i)$ for the three SH modes, where $i = 1$, 2, and 3. These values are used to evaluate the optical field quadrature variances for the propagating modes $\left\langle(\Delta\hat{X}_j)^2\right\rangle$, $\left\langle(\Delta\hat{Y}_j)^2\right\rangle$ using Eq. (32). For the analytical method, the numerical procedure involves two main steps – viz. (i) solving simultaneously the coupled sets of Eqs. (A1)–(A48) to obtain numerical values of the time-dependent coefficients $\{\boldsymbol{A}_k(t)\}_1^{10}$, $\{\boldsymbol{B}_k(t)\}_1^{10}$, $\{\boldsymbol{C}_k(t)\}_1^{10}$, $\{\boldsymbol{D}_k(t)\}_1^{6}$, $\{\boldsymbol{E}_k(t)\}_1^{6}$ and $\{\boldsymbol{F}_k(t)\}_1^{6}$, and (ii) with the knowledge of these coefficients, the optical field quadrature variances for the propagating modes $\left\langle(\Delta\hat{X}_j)^2\right\rangle$, $\left\langle(\Delta\hat{Y}_j)^2\right\rangle$ can be evaluated using Eqs. (33)–(35). It should be emphasized that (α_i, β_i) and $(\bar{\alpha}_i, \bar{\beta}_i)$ are time-dependent in the phase-space method, whereas they are time-independent in the analytical method. Finally, for the convenience of numerical simulation, dimensionless input parameters are used. For the codirectional system, the relevant systems of Eqs. (5)–(16) and (A1)–(A48) are scaled with respect to the input frequency of the first mode (ω_1), such that $\tilde{\omega}_1 = \frac{\omega_1}{\omega_1} = 1$, $\tilde{\omega}_2 = \frac{\omega_2}{\omega_1}$, $\tilde{\omega}_3 = \frac{\omega_3}{\omega_1}$, $\tilde{g} = \frac{g}{\omega_1}$, $\tilde{\kappa} = \frac{\kappa}{\omega_1}$, $\tau = \omega_1 t$ and $\tilde{\eta}(\tau) = \frac{\eta(t)}{\sqrt{\omega_1}}$. For The contra-directional case, the spatial system (36)–(47) can be scaled with the wavenumber of the first mode k_1 using the dimensionless parameters, $\tilde{k}_1 = \frac{k_1}{k_1} = 1$, $\tilde{k}_2 = \frac{k_2}{k_1}$, $\tilde{k}_3 = \frac{k_3}{k_1}$, $\tilde{G} = \frac{G}{k_1}$, $\tilde{K} = \frac{K}{k_1}$, $\tilde{z} = k_1 z$ and $\tilde{\xi}_l = \frac{\xi_l}{\sqrt{k_1}}$. This will produce a dimensionless form of the spatial system (36)–(47).

3 Result and discussion

We begin this section by looking at the evolution of the field quadrature variances at various initial input field amplitudes. Other input parameters are fixed, with the nonlinear coupling coefficient of $\tilde{g}$ set to 0.01 and the linear coupling $\tilde{\kappa}$ to 0.1. likewise, the frequency of propagating modes is fixed at $\tilde{\omega}_1 = \tilde{\omega}_2 = \tilde{\omega}_3 = 1$. In Fig. 2, We focus on the case that the initial amplitudes of the input fields in the three waveguides are equal; this is known as symmetric initialization (where $\alpha_1 = \alpha_2 = \alpha_3 = 1$). Under this combination of input values, both methods yield a continuous oscillation pattern. Squeezing in the first, second, and third modes is found to be identical, with all three modes exhibiting the same degree and duration of long-lasting squeezing. Therefore, only the squeezed states generated in one channel are shown in Fig. 2 and subsequent figures. At the earlier stages of evolution, until $\tau \sim 4$ both methods acquire a high degree of agreement. Whereas, as time passes, the phase space method predicts a lower amplitude for the field quadratures than the AP

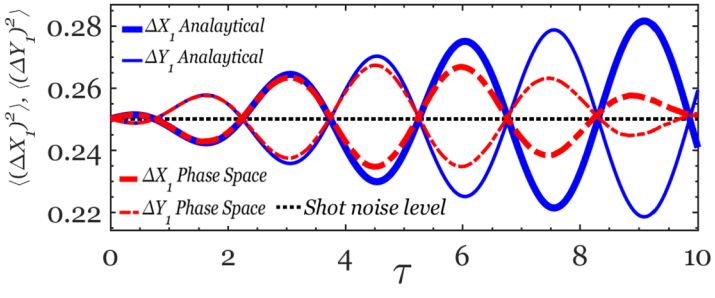

Figure 2 Evolution of squeezing for mode $\hat{E}_1$ with $\alpha_1 = \alpha_2 = \alpha_3 = 1$, $\tilde{\omega}_1 = \tilde{\omega}_2 = \tilde{\omega}_3 = 1$, $\tilde{g} = 0.01$ and $\tilde{\kappa} = 0.1$

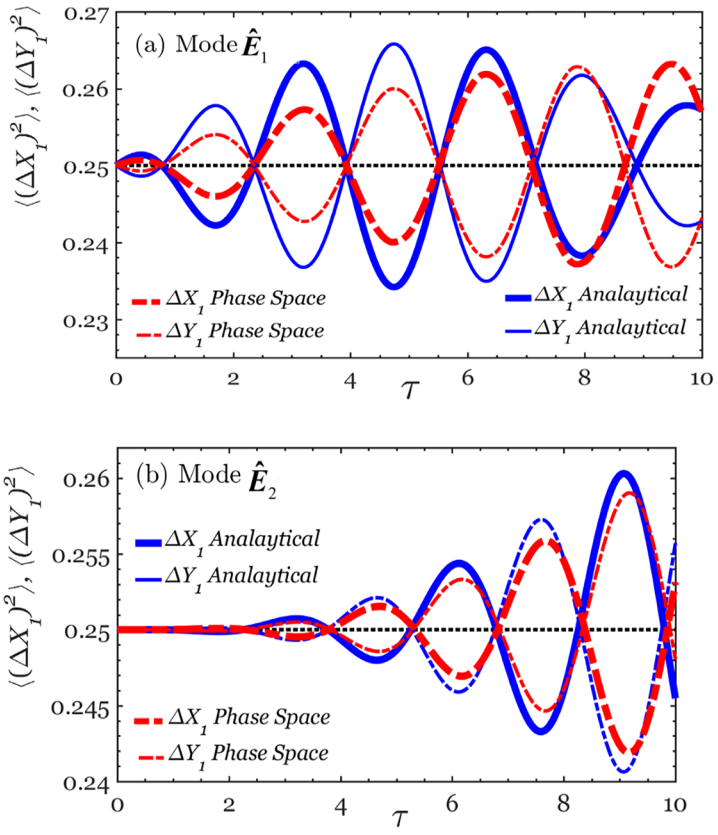

Figure 3 Fluctuation of squeezing for (a) coherent-mode $\hat{E}_1$, (b) vacuum-mode $\hat{E}_2$ with $\alpha_1 = 1, \alpha_2 = \alpha_3 = 0$, $\tilde{\omega}_1 = \tilde{\omega}_2 = \tilde{\omega}_3 = 1$, $\tilde{g} = 0.01$ and $\tilde{\kappa} = 0.1$

method. Despite this, both systems display signals that are completely in phase. However, the constant increase in field amplitude found by the AP method over time does not appear reasonable. This indicates that, under symmetric initialization of the system, the AP method provides reasonable results only during the early stages of evolution. Moreover, the accuracy of this range appears to depend on the specific combination of input parameters used.

In Fig. 3, the results are obtained by initializing the system with a single coherent mode ($\alpha_1 = 1$) and vacuum states for the rest ($\alpha_2 = \alpha_3 = 0$); this is known as asymmetric initialization. Additional input parameters are maintained in the same manner as in Fig. 2. Figure 3(a) depicts the squeezing generated by the mode initiated by a coherent mode, while Fig. 3(b) illustrates the squeezing generated by the second mode ($\hat{E}_2$) initiated by a vacuum state. The third mode ($\hat{E}_3$) exhibits similar behavior to $\hat{E}_2$ and is therefore not shown to avoid repetition. This means that with a single coherent light source, the system can generate squeezed light from all three waveguides. This capability to produce multiple squeezed outputs from a single source is a significant feature of a multiple-waveguide device. Regarding the coherent mode, both methods are nearly in total agreement and sufficiently in phase for lengthy periods (up to $\tau \approx 7$). After that, discrepancies between both methods start appearing. Nevertheless, modes prepared in vacuum states have shown an excellent agreement for longer evolution distances, as shown in Fig. 3(b) for vacuum mode $\hat{E}_2$. Similar results were obtained for the vacuum mode $\hat{E}_3$. This supports our hypothesis

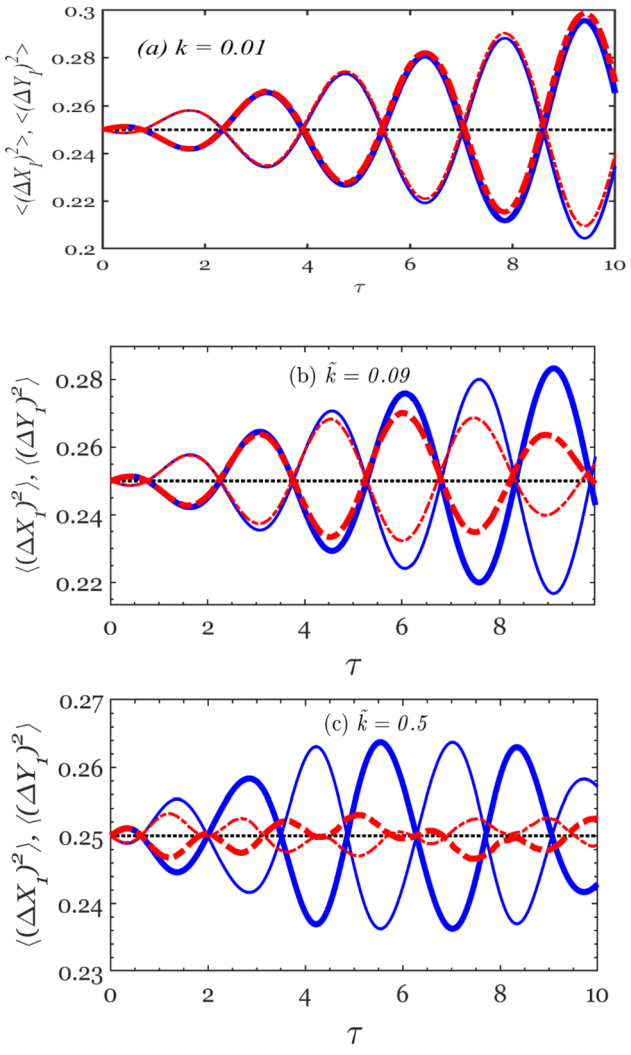

Figure 4 Squeezing in mode $\hat{E}_1$ for (a) $\tilde{\kappa} = 0.01$, (b) $\tilde{\kappa} = 0.09$ and (c) $\tilde{\kappa} = 0.5$ with $\alpha_1 = \alpha_2 = \alpha_3 = 1$, $\tilde{\omega}_1 = \tilde{\omega}_2 = \tilde{\omega}_3 = 1$ and $\tilde{g} = 0.01$

that the AP method performs well during the early stages of evolution and for low values of input parameters, even under asymmetric initialization. However, both methods demonstrate the general trend of oscillatory squeezed states, and both detect the same form of long-lasting oscillatory squeezed states.

We now examine the effects of different linear coupling strengths on squeezing. In practice, this parameter can be manipulated by altering the distance between channel waveguides. It is possible to enhance the linear coupling constant by bringing the channel waveguides closer together, and vice versa. Figure 4(a), 4(b), and 4(c) depict the outcomes for scaled linear coupling strength of $\tilde{\kappa} = 0.01$, $\tilde{\kappa} = 0.09$ and $\tilde{\kappa} = 0.5$, respectively. To generate these results, all modes are prepared in coherent states with $\alpha_1 = \alpha_2 = \alpha_3 = 1$ (symmetric initialization) and a common frequency $\tilde{\omega}_1 = \tilde{\omega}_2 = \tilde{\omega}_3 = 1$. In addition, the nonlinear coupling constant is set to $\tilde{g} = 0.01$. Here, we present the outcome for the first mode only since the other two modes generate exactly similar results. At $\tilde{\kappa} = 0.01$ (Fig. 4(a)), both methods are totally in-phase and completely agree with one another till $\tau \sim 10$; however, at

$\tilde{\kappa}$ = 0.09, the agreement in maximal amplitude is only maintained up to $\tau \sim 4$ (Fig. 4(b)). When $\tilde{\kappa}$ = 0.5 (Fig. 4(c)), the results obtained from the phase space method and the AP method are different; the phase space method generates collapses-revivals behaviour with a small amplitude, whereas the AP method predicts a very high squeezing amplitude. In this case, the highest level of agreement is only reached during the earliest phases of evolution up to $\tau \sim 1$ only. In summary, for symmetric initialization, the discrepancy in the field amplitude detected by both methods increases as the linear coupling coefficients increase. This is because, for higher values of the linear couplings, the AP method begins to deviate at shorter time scales. However, both methods agree on the generation of a long-lasting squeezing that goes much further beyond τ = 10 from the current three-waveguide system.

Figure 5 shows squeezing induced at different values of linear coupling constant ($\tilde{k}$), as those in Fig. 4. Here, however, the first waveguide is prepared in a coherent state with magnitude α_1 = 1 while the second and the third waveguided are initially prepared in vacuum states with $\alpha_2 = \alpha_3 = 0$ (asymmetric initialization). We just consider the squeezing caused by the coherent mode $\hat{E}_1$. Other modes show squeezed states similar to those produced in Fig. 3b. At $\tilde{\kappa}$ = 0.01 (Fig. 5(a)), the observed results are comparable to those in Fig. 4(a).

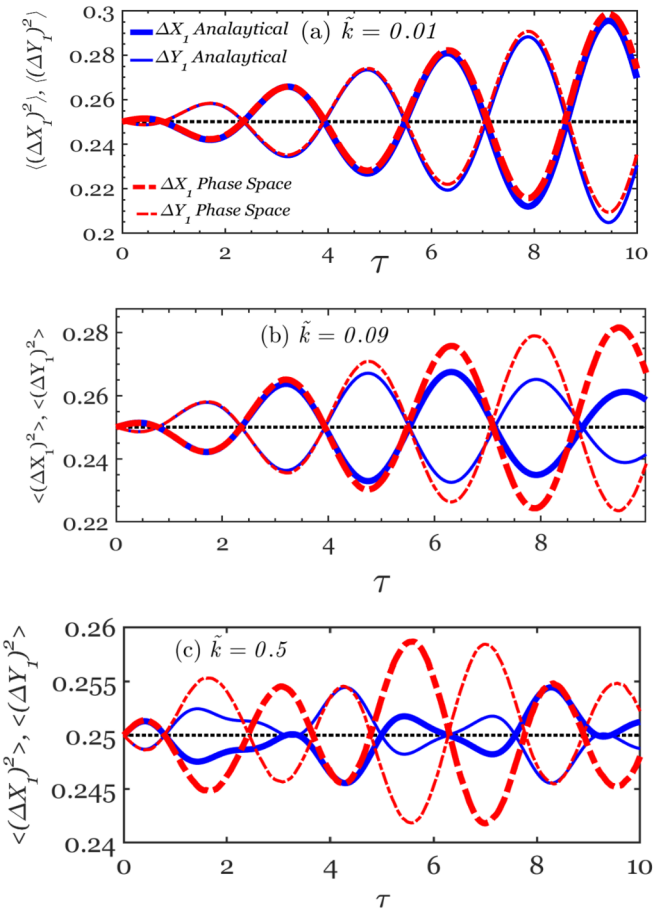

Figure 5 Single-mode squeezing in coherent-mode $\hat{E}_1$ for (a) $\tilde{\kappa}$ = 0.01, (b) $\tilde{\kappa}$ = 0.09 and (c) $\tilde{\kappa}$ = 0.5 with $\alpha_1 = 1, \alpha_2 = \alpha_3 = 0, \tilde{\omega}_1 = \tilde{\omega}_2 = \tilde{\omega}_3 = 1$ and $\tilde{g} = 0.01$

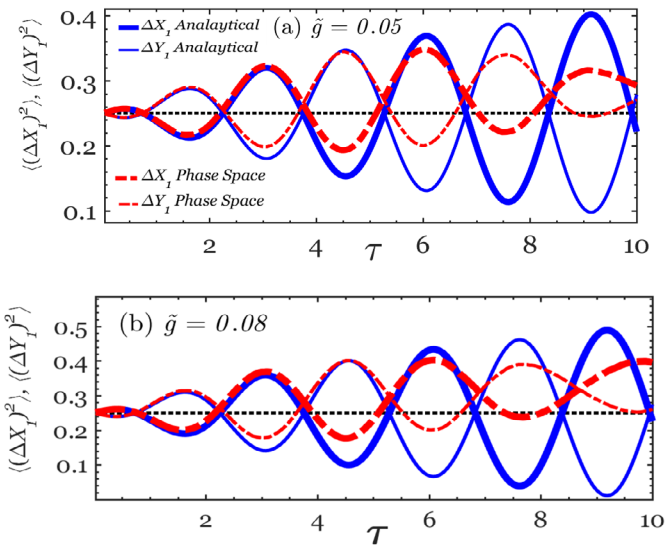

Figure 6 Variation of squeezing in mode $\hat{E}_1$ for (a) $\tilde{g} = 0.05$ and (b) $\tilde{g} = 0.08$ with $\alpha_1 = \alpha_2 = \alpha_3 = 1$, $\tilde{\omega}_1 = \tilde{\omega}_2 = \tilde{\omega}_3 = 1$ and $\tilde{\kappa} = 0.1$

This similarity may be attributable to the negligible levels of linear coupling strength. At $\tilde{\kappa} = 0.09$ (Fig. 5(b)), both approaches generate comparable stable oscillation patterns, however, at $\tilde{\kappa} = 0.5$ (Fig. 5(c)), the oscillation of squeezing is no longer continuous, and a pattern of mild collapses and revivals is observed. In addition, a large value of $\tilde{\kappa}$ produces a squeezing with substantial oscillatory quadrature fluctuations, as shown in Fig. 4(c) and 5(c). In summary, for asymmetric initialization, the discrepancy in the detected field amplitude between the two methods increases as the linear coupling coefficients increase. However, both methods agree on the detection of long-lasting squeezing that goes beyond $\tau = 10$. This long-lasting squeezing is useful in various potential applications such as gravitational-wave observatories, quantum information protocols, quantum metrology, and neuromorphic machine learning [54].

Next, we investigate the influence of nonlinear coupling on the generated squeezed light in the current system. Figures 6 and 7, respectively, depict this for the symmetrical and asymmetrical initializations. Figure 6(a) and (b) illustrate the squeezing produced at two distinct values of coupling coefficient, viz. $\tilde{g} = 0.05$ (Fig. 6(a)) and $\tilde{g} = 0.08$ (Fig. 6(b)). As shown in Fig. 6, both the values of $\tilde{g}$ yield two patterns with similar characteristics. Yet, the maximal squeezing amplitude appears to be greater at $\tilde{g} = 0.08$ than at $\tilde{g} = 0.05$. Hence, the squeezed signal becomes increasingly significant as the nonlinear coupling increases. Beginning at a specific time ($\tau \approx 8$), the squeezing signal disappears in the phase space. Figure 7 examines the effect of nonlinear coupling in the situation of asymmetrical initialization; the first waveguide is prepared in a coherent state while the other two waveguides are prepared in vacuum states. Like the values used in Fig. 6, squeezing is examined at $\tilde{g} = 0.05$ and $\tilde{g} = 0.08$ (Fig. 7(a) and (b) correspondingly). As anticipated, both values of the nonlinear coefficient result in the same degree of squeezing. In this case, a strong signal of squeezing is also noticed when $g = 0.08$ rather than $g = 0.05$. In conclusion, the intensity of the squeezing grows as the nonlinear coupling rises. In summary, here for both symmetric and asymmetric initialization, the discrepancy in the detected field amplitude between

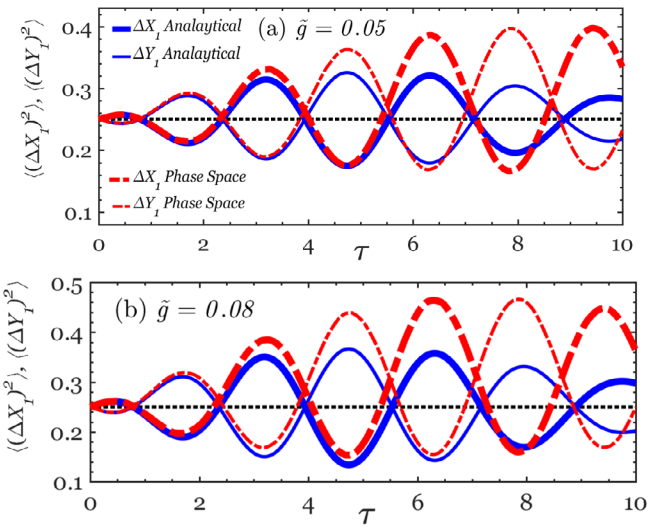

Figure 7 Variation of quadrature variances in coherent-mode $\hat{E}_1$ for (a) $\tilde{g} = 0.05$ and (b) $\tilde{g} = 0.08$ with $\alpha_1 = 1$, $\alpha_2 = \alpha_3 = 0$, $\tilde{\omega}_1 = \tilde{\omega}_2 = \tilde{\omega}_3 = 1$ and $\tilde{\kappa} = 0.1$

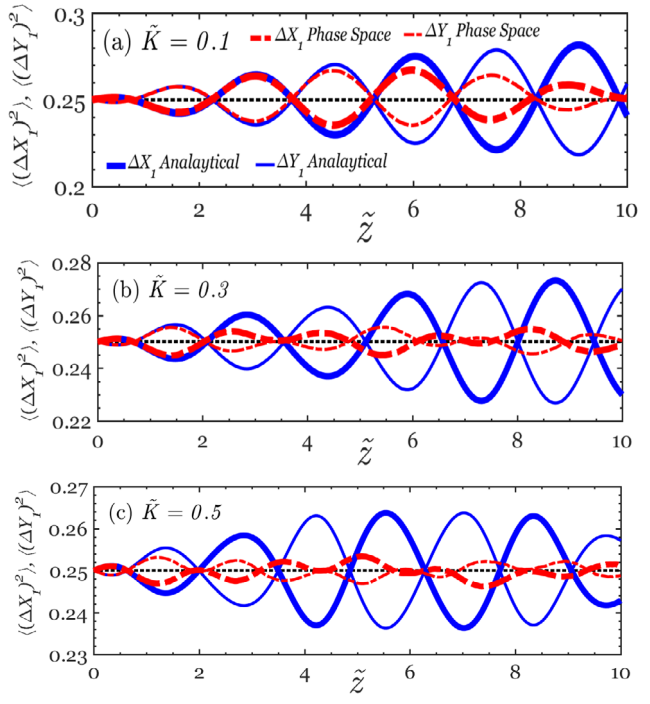

Figure 8 Variation of squeezing in mode $\hat{E}_1$ as a function of scaled distance $\tilde{Z}$ for (a) $\tilde{K} = 0.1$, (b) $\tilde{K} = 0.3$ and (b) $\tilde{K} = 0.5$ with $\alpha_1 = \alpha_2 = \alpha_3 = 1$, $\tilde{k}_1 = \tilde{k}_2 = \tilde{k}_3 = 1$ and $\tilde{G} = 0.01$

the two methods increases over time. However, both methods agree on the detection of the same range of squeezing.

Finally, we will present our observation when from the contra-directional propagation. In this case, the second mode is set to be propagating in the opposite direction to the other modes. In Fig. 8, the system is initialized symmetrically with all modes having the same

amplitude of $\alpha = 1$, and a common wavenumber, $\tilde{k} = 1$. The nonlinear coupling constant is set to be $\tilde{G} = 0.01$, while the linear coupling constant is varied as $\tilde{K} = 0.1$ (Fig. 8(a)), $\tilde{K} = 0.3$ (Fig. 8(b)) and $\tilde{K} = 0.5$ (Fig. 8(c)). As in the codirectional setup, the phase space method agrees very well with the analytical method at early evolution distances. The agreement lasts longer at lower values of the linear couplings (Fig. 8(a)). Another noticeable difference is that for the phase space method, squeezing with steady oscillation is observed at $\tilde{K} = 0.1$. When $\tilde{K}$ increases, the signal becomes lower in amplitude at certain wave periods, perhaps due to some kind of destructive interference. Oppositely, the AP method remains less sensitive to the contra-directional arrangement with steady fluctuation of squeezing at $\hat{K} = 0.1$ and $\hat{K} = 0.3$, but showing mild collapses and revivals type of pattern at $\hat{K} = 0.5$. The contra-directional case could be advantageous for adiabatically controlling light, where the quantum state remains in its instantaneous eigenstate if perturbations are applied slowly enough. This allows for smooth transitions between different modes or states without abrupt changes. For instance, by designing the coupler system parameters to achieve adiabatic evolution, contra-directional light propagation can be effectively managed, ensuring precise control over light behaviors such as transfer, splitting, and returning. The ability to control light propagation through adiabatic processes in nonlinear regimes opens new avenues for developing high-fidelity integrated optical devices capable of performing complex operations with minimal loss and high precision.

4 Conclusion

The squeezed state of light generated in a three-waveguide nonlinear coupler with SH generation has been studied using both the phase space and the AP method. Rather than depending on a single theoretical prediction, both methods have been used to investigate the squeezed states of light propagating in the current system to ensure accurate findings and to provide insights into the strengths and weaknesses of each method. The impact of key design parameters on generated squeezed states was investigated under various conditions, including full frequency matching, symmetrical and asymmetrical waveguide initialization, and both codirectional and contradirectional propagation. The system consistently produced long-lasting squeezed states across all three waveguides, even with asymmetrical initialization. Specifically, for symmetrical initialization, where all waveguides are driven by a coherent light source, identical and enduring squeezing was achieved in each waveguide. When only one waveguide was pumped while the other two were initialized in the vacuum state, long-lasting squeezing in all waveguides was still observed due to energy exchange between them. This demonstrates that a single coherent light source can effectively generate squeezed light in all three waveguides, highlighting a significant feature of the system. Moreover, the squeezing effect was found to persist for an extended duration in nearly all simulated scenarios, enhancing the system's practical utility, particularly for applications requiring long-range squeezed light.

At low values of linear coupling, both methods are in-phase and completely agree with one another. When the linear coupling increases, results obtained exploiting the two approaches differ; the phase space method generates collapses-revivals behavior with a small amplitude, whereas the analytical method predicts a constant increase in the field amplitude. The agreement between the two methods decreases as the linear coupling coefficients are raised in both codirectional and contra-directional systems. In addition, a

stronger linear coupling produces a squeezing with substantial oscillatory quadrature fluctuations. As the nonlinear coupling increases, the degree of squeezing is significantly enhanced. However, this comes at the expense of squeezing range over time. Generally, the AP method yields similar performance to the phase space positive-P method for low-input parameters and short periods of evolution. In fact, at certain combinations of design parameters, the analytical method exhibits a constant increase in field amplitude over time which does not appear reasonable. While we think that the positive-P phase space method yields more accurate results, the analytical method could be used for short evolution distances and as a verification of the overall results. This work opens a new avenue for utilizing multi-waveguide NLC in nonclassical light generation in the new era of quantum-based technology.

Appendix A

The time-dependent coefficients $\{\boldsymbol{A}_k(t)\}_1^{10}$, $\{\boldsymbol{B}_k(t)\}_1^{10}$, $\{\boldsymbol{C}_k(t)\}_1^{10}$, $\{\boldsymbol{D}_k(t)\}_1^{6}$, $\{\boldsymbol{E}_k(t)\}_1^{6}$ and $\{\boldsymbol{F}_k(t)\}_1^{6}$ appears in the solutions given in (25)–(30) of the AP method, are evaluated precisely by substituting the previous solutions (25)–(30) back into the evolution Eqs. (18)–(23) and equating similar terms on both sides. The sets of coupled equations representing the evolution of these coefficients are obtained as follows.

The evolution of the $\{\boldsymbol{A}_k\}_1^{10}$ for fundamental operator $\hat{a}_1$

$$\frac{d\,\mathrm{A}_1}{dt} = -i\omega_1\,\mathrm{A}_1 - ik\,\mathrm{B}_1 - ik\,\mathrm{C}_1 \tag{A1}$$

$$\frac{d\,\mathrm{A}_2}{dt} = -i\omega_1\,\mathrm{A}_2 - ik\,\mathrm{B}_2 - ik\,\mathrm{C}_2 \tag{A2}$$

$$\frac{d\,\mathrm{A}_3}{dt} = -i\omega_1\,\mathrm{A}_3 - ik\,\mathrm{B}_3 - ik\,\mathrm{C}_3 \tag{A3}$$

$$\frac{d\,\mathrm{A}_4}{dt} = -i\omega_1\,\mathrm{A}_4 + g\,\mathrm{A}_1^*\,\mathrm{D}_1 - ik\,\mathrm{B}_5 - ik\,\mathrm{C}_6 \tag{A4}$$

$$\frac{d\,\mathrm{A}_5}{dt} = -i\omega_1\,\mathrm{A}_5 - ik\,\mathrm{B}_6 - ik\,\mathrm{C}_5 \tag{A5}$$

$$\frac{d\,\mathrm{A}_6}{dt} = -i\omega_1\,\mathrm{A}_6 - ik\,\mathrm{B}_7 - ik\,\mathrm{C}_7 \tag{A6}$$

$$\frac{d\,\mathrm{A}_7}{dt} = -i\omega_1\,\mathrm{A}_7 + g\,\mathrm{A}_2^*\,\mathrm{D}_1 \tag{A7}$$

$$\frac{d\,\mathrm{A}_8}{dt} = -i\omega_1\,\mathrm{A}_8 + g\,\mathrm{A}_3^*\,\mathrm{D}_1 \tag{A8}$$

$$\frac{d\,\mathrm{A}_9}{dt} = -i\omega_1\,\mathrm{A}_9 + g\,\mathrm{A}_4^*\,\mathrm{D}_1 \tag{A9}$$

$$\frac{d\,\mathrm{A}_{10}}{dt} = -i\omega_1\,\mathrm{A}_{10} + g\,\mathrm{A}_1^*\,\mathrm{D}_2 \tag{A10}$$

The evolution of the $\{\boldsymbol{B}_k\}_1^{10}$ for fundamental operator $\hat{a}_2$

$$\frac{d\,\mathrm{B}_1}{dt} = -i\omega_2\,\mathrm{B}_1 - ik\,\mathrm{A}_1 - ik\,\mathrm{C}_1 \tag{A11}$$

$$\frac{d\,\mathrm{B}_2}{dt} = -i\omega_2\,\mathrm{B}_2 - ik\,\mathrm{A}_2 - ik\,\mathrm{C}_2 \tag{A12}$$

$$\frac{d\,\mathrm{B}_3}{dt} = -i\omega_2\,\mathrm{B}_3 - ik\,\mathrm{A}_3 - ik\,\mathrm{C}_3 \tag{A13}$$

$$\frac{d\,\mathrm{B}_4}{dt} = -i\omega_2\,\mathrm{B}_4 + g\,\mathrm{B}_1^*\,\mathrm{E}_1 \tag{A14}$$

$$\frac{d\,\mathrm{B}_5}{dt} = -i\omega_2\,\mathrm{B}_5 - ik\,\mathrm{A}_4 - ik\,\mathrm{C}_6 \tag{A15}$$

$$\frac{d\,\mathrm{B}_6}{dt} = -i\omega_2\,\mathrm{B}_6 + g\,\mathrm{B}_2^*\,\mathrm{E}_1 - ik\,\mathrm{A}_5 - ik\,\mathrm{C}_5 \tag{A16}$$

$$\frac{d\,\mathrm{B}_7}{dt} = -i\omega_2\,\mathrm{B}_7 - ik\,\mathrm{A}_6 - ik\,\mathrm{C}_7 \tag{A17}$$

$$\frac{d\,\mathrm{B}_8}{dt} = -i\omega_2\,\mathrm{B}_8 + g\,\mathrm{B}_3^*\,\mathrm{E}_1 \tag{A18}$$

$$\frac{d\,\mathrm{B}_9}{dt} = -i\omega_2\,\mathrm{B}_9 + g\,\mathrm{B}_6^*\,\mathrm{E}_1 \tag{A19}$$

$$\frac{d\,\mathrm{B}_{10}}{dt} = -i\omega_2\,\mathrm{B}_{10} + g\,\mathrm{B}_2^*\,\mathrm{E}_2 \tag{A20}$$

The evolution of the $\{\boldsymbol{C}_k\}_1^{10}$ for fundamental operator $\hat{a}_3$

$$\frac{d\,\mathrm{C}_1}{dt} = -i\omega_3\,\mathrm{C}_1 - ik\,\mathrm{B}_1 - ik\,\mathrm{A}_1 \tag{A21}$$

$$\frac{d\,\mathrm{C}_2}{dt} = -i\omega_3\,\mathrm{C}_2 - ik\,\mathrm{B}_2 - ik\,\mathrm{A}_2 \tag{A22}$$

$$\frac{d\,\mathrm{C}_3}{dt} = -i\omega_3\,\mathrm{C}_3 - ik\,\mathrm{B}_3 - ik\,\mathrm{A}_3 \tag{A23}$$

$$\frac{d\,\mathrm{C}_4}{dt} = -i\omega_3\,\mathrm{C}_4 + g\,\mathrm{C}_1^*\,\mathrm{F}_1 \tag{A24}$$

$$\frac{d\,\mathrm{C}_5}{dt} = -i\omega_3\,\mathrm{C}_5 - ik\,\mathrm{B}_6 - ik\,\mathrm{A}_5 \tag{A25}$$

$$\frac{d\,\mathrm{C}_6}{dt} = -i\omega_3\,\mathrm{C}_6 - ik\,\mathrm{B}_5 - ik\,\mathrm{A}_4 \tag{A26}$$

$$\frac{d\,\mathrm{C}_7}{dt} = -i\omega_3\,\mathrm{C}_7 + g\,\mathrm{C}_3^*\,\mathrm{F}_1 - ik\,\mathrm{B}_7 - ik\,\mathrm{A}_6 \tag{A27}$$

$$\frac{d\,\mathrm{C}_8}{dt} = -i\omega_3\,\mathrm{C}_8 + g\,\mathrm{C}_7^*\,\mathrm{F}_1 \tag{A28}$$

$$\frac{d\,\mathrm{C}_9}{dt} = -i\omega_3\,\mathrm{C}_9 + g\,\mathrm{C}_2^*\,\mathrm{F}_1 \tag{A29}$$

$$\frac{d\,\mathrm{C}_{10}}{dt} = -i\omega_3\,\mathrm{C}_{10} + g\,\mathrm{C}_3^*\,\mathrm{F}_4 \tag{A30}$$

The evolution of the $\{\boldsymbol{D}_k(t)\}_1^6$ for the first harmonic operator $\hat{b}_1$

$$\frac{d\,\mathrm{D}_1}{dt} = -i\,(2\omega_1)\,\mathrm{D}_1 \tag{A31}$$

$$\frac{d\,\mathrm{D}_2}{dt} = -i\,(2\omega_1)\,\mathrm{D}_2 - \frac{g}{2}\,\mathrm{A}_1^2 \tag{A32}$$

$$\frac{d\,\mathrm{D}_3}{dt} = -i\,(2\omega_1)\,\mathrm{D}_3 - g\,\mathrm{A}_1\,\mathrm{A}_2 \tag{A33}$$

$$\frac{d\,\mathrm{D}_4}{dt} = -i\,(2\omega_1)\,\mathrm{D}_4 - g\,\mathrm{A}_1\,\mathrm{A}_3 \tag{A34}$$

$$\frac{d\,\mathrm{D}_5}{dt} = -i\,(2\omega_1)\,\mathrm{D}_5 - \frac{g}{2}\,\mathrm{A}_4\,\mathrm{A}_1 \tag{A35}$$

$$\frac{d\,\mathrm{D}_6}{dt} = -i\,(2\omega_1)\,\mathrm{D}_6 - \frac{g}{2}\,\mathrm{A}_1\,\mathrm{A}_4 \tag{A36}$$

The evolution of the $\{\boldsymbol{E}_k(t)\}_1^6$ for the SH operator $\hat{b}_2$

$$\frac{d\,\mathrm{E}_1}{dt} = -i\,(2\omega_2)\,\mathrm{E}_1 \tag{A37}$$

$$\frac{d\,\mathrm{E}_2}{dt} = -i\,(2\omega_2)\,\mathrm{E}_2 - \frac{g}{2}\,\mathrm{B}_2^2 \tag{A38}$$

$$\frac{d\,\mathrm{E}_3}{dt} = -i\,(2\omega_2)\,\mathrm{E}_3 - g\,\mathrm{B}_1\,\mathrm{B}_2 \tag{A39}$$

$$\frac{d\,\mathrm{E}_4}{dt} = -i\,(2\omega_2)\,\mathrm{E}_4 - g\,\mathrm{B}_2\,\mathrm{B}_3 \tag{A40}$$

$$\frac{d\,\mathrm{E}_5}{dt} = -i\,(2\omega_2)\,\mathrm{E}_5 - \frac{g}{2}\,\mathrm{B}_6\,\mathrm{B}_2 \tag{A41}$$

$$\frac{d\,\mathrm{E}_6}{dt} = -i\,(2\omega_2)\,\mathrm{E}_6 - \frac{g}{2}\,\mathrm{B}_2\,\mathrm{B}_6 \tag{A42}$$

The evolution of the $\{\boldsymbol{F}_k(t)\}_1^6$ for the third harmonic operator $\hat{b}_3$

$$\frac{d\,\mathrm{F}_1}{dt} = -i\,(2\omega_3)\,\mathrm{F}_1 \tag{A43}$$

$$\frac{d\,\mathrm{F}_2}{dt} = -i\,(2\omega_3)\,\mathrm{F}_2 - g\,\mathrm{C}_2\,\mathrm{C}_3 \tag{A44}$$

$$\frac{d\,\mathrm{F}_3}{dt} = -i\,(2\omega_3)\,\mathrm{F}_3 - g\,\mathrm{C}_1\,\mathrm{C}_3 \tag{A45}$$

$$\frac{d\,\mathrm{F}_4}{dt} = -i\,(2\omega_3)\,\mathrm{F}_4 - \frac{g}{2}\,\mathrm{C}_3^2 \tag{A46}$$

$$\frac{d\,\mathrm{F}_5}{dt} = -i\,(2\omega_3)\,\mathrm{F}_5 - \frac{g}{2}\,\mathrm{C}_7\,\mathrm{C}_3 \tag{A47}$$

$$\frac{d\,\mathrm{F}_6}{dt} = -i\,(2\omega_3)\,\mathrm{F}_6 - \frac{g}{2}\,\mathrm{C}_3\,\mathrm{C}_7 \tag{A48}$$

Appendix B

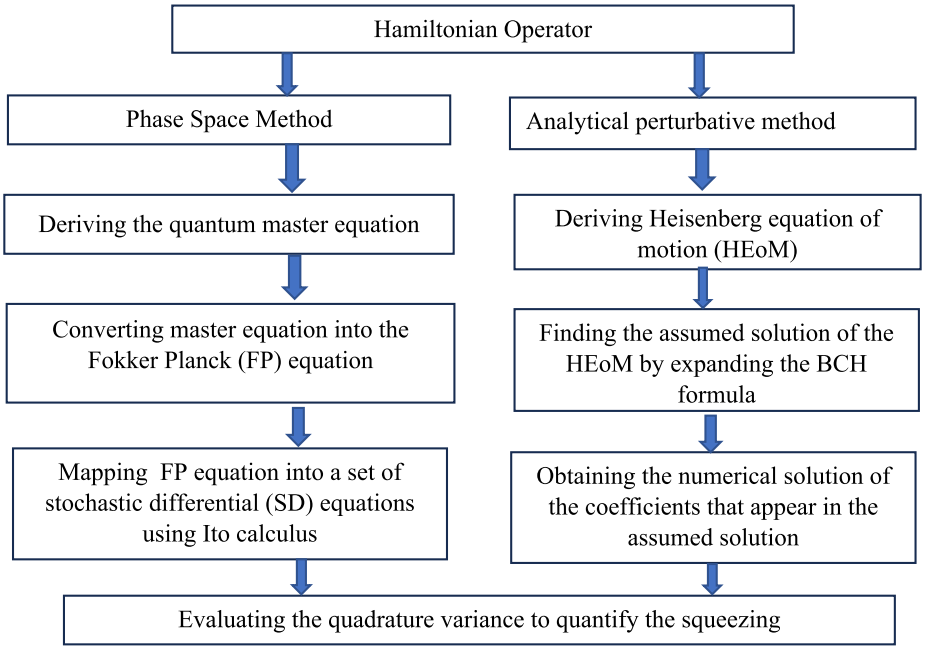

Figure 9 A flowchart outlining the steps of the mathematical process for both the phase space method and the analytical perturbative method

Acknowledgements
Not applicable

Author contributions
The main idea, mathematical derivation, numerical simulation, and results were contributed by M.S.M.H, A.M.A.I., and R.J respectively. while A.M.A.I., P.K.C. and H. E. looked over the entire study and the manuscript preparation.

Funding
R Julius gratefully recognizes the Malaysian Ministry of Higher Education (MOHE) national grant FRGS/1/2021/STG07/UITM/02/4.

Availability of data and materials
A MATLAB code was developed to generate these theoretical results. The code is available from the corresponding author upon reasonable request.

Declarations

Competing interests
The authors declare no competing interests.

Author details
[1]Faculty of Applied Sciences, Universiti Teknologi MARA (UiTM), 40450 Shah Alam, Selangor, Malaysia. [2]Faculty of Applied Sciences, Universiti Teknologi MARA (UiTM) Perak, Tapah Campus, Perak, Malaysia. [3]International Research Center for Advanced Photonics, Zhejiang University, Building 1A, 718 East Haizhou Rd., Haining, Zhejiang 314400, P.R. China. [4]Department of Applied Physics and Astronomy, University of Sharjah, Sharjah, United Arab Emirates. [5]College of Arts and Sciences, Abu Dhabi University, Abu Dhabi 59911, United Arab Emirates.

Received: 27 April 2023 Accepted: 5 August 2024 Published online: 14 August 2024

References

1. Ficek Z, Wahiddin MR. Quantum optics for beginners. 1st ed. New York: Jenny Stanford Publishing; 2016.
2. Giovannetti V, Lloyd S, Maccone L. Quantum-enhanced measurements: beating the standard quantum limit. Science. 2004;306:1330–6.

3. Li Y-M, Wang X-Y, Bai Z-L, Liu W-Y, Yang S-S, Peng K-C. Continuous variable quantum key distribution. Chin Phys B. 2017;26:040303.
4. Schlegel DS, Minganti F, Savona V. Quantum error correction using squeezed Schrödinger cat states. Phys Rev A. 2022;106:022431.
5. Menicucci NC, Van Loock P, Gu M, Weedbrook C, Ralph TC, Nielsen MA. Universal quantum computation with continuous-variable cluster states. Phys Rev Lett. 2006;97:110501.
6. Tse M, Yu H, Kijbunchoo N, Fernandez-Galiana A, Dupej P, Barsotti L, et al. Quantum-enhanced advanced LIGO detectors in the era of gravitational-wave astronomy. Phys Rev Lett. 2019;123:231107.
7. Gottesman D, Secure PJ. Quantum key distribution using squeezed states. In: Braunstein SL, Pati AK, editors. Quantum inf contin var. Dordrecht: Springer Netherlands; 2003. p. 317–56.
8. Gatti A, Brambilla E, Lugiato L. Quantum imaging. Prog Opt. 2008;51:251–348.
9. Masada G. Two-mode squeezed light source for quantum illumination and quantum imaging. In: Quantum commun quantum imaging XIII. Bellingham: SPIE; 2015. p. 7–15.
10. Casacio CA, Madsen LS, Terrasson A, Waleed M, Barnscheidt K, Hage B, et al. Quantum-enhanced nonlinear microscopy. Nature. 2021;594:201–6.
11. Taylor MA, Janousek J, Daria V, Knittel J, Hage B, Bachor H-A, et al. Biological measurement beyond the quantum limit. Nat Photonics. 2013;7:229–33.
12. Politi A, Matthews JC, Thompson MG, O'Brien JL. Integrated quantum photonics. IEEE J Sel Top Quantum Electron. 2009;15:1673–84.
13. Messin G, Karr JP, Eleuch H, Courty J-M, Giacobino E. Squeezed states and the quantum noise of light in semiconductor microcavities. J Phys Condens Matter. 1999;11:6069.
14. Andersen UL, Gehring T, Marquardt C, Leuchs G. 30 years of squeezed light generation. Phys Scr. 2016;91:053001.
15. Qasymeh M, Eleuch H. Hybrid two-mode squeezing of microwave and optical fields using optically pumped graphene layers. Sci Rep. 2020;10:16676.
16. Eleuch H. Noise spectra of microcavity-emitting field in the linear regime. Eur Phys J D. 2008;49:391–5.
17. Breunig I. Three-wave mixing in whispering gallery resonators. Laser Photonics Rev. 2016;10:569–87.
18. Solntsev AS, Sukhorukov AA. Path-entangled photon sources on nonlinear chips. Rev Phys. 2017;2:19–31.
19. Marshall GD, Politi A, Matthews JC, Dekker P, Ams M, Withford MJ, et al. Laser written waveguide photonic quantum circuits. Opt Express. 2009;17:12546–54.
20. Politi A, Matthews JC, Thompson MG, O'Brien JL. Integrated quantum photonics. IEEE J Sel Top Quantum Electron. 2009;15:1673–84.
21. Julius R, Zahirzai M, Ibrahim A-BMA, Eleuch H, Choudhury PK. Single- and compound-mode squeezing in nonlinear coupler with frequency mismatch. J Electromagn Waves Appl. 2019;34:1–15.
22. Korolkova N, Peřina J. Quantum statistics and dynamics of Kerr nonlinear couplers. Opt Commun. 1997;136:135–49.
23. Mandal S, Perina J. Approximate quantum statistical properties of a nonlinear optical coupler. Phys Lett A. 2004;328:144–56.
24. Zhang Y, McKnight L, Engin E, Watson IM, Cryan MJ, Gu E, et al. GaN directional couplers for integrated quantum photonics. Appl Phys Lett. 2011;99:161119.
25. Li HW, Przeslak S, Niskanen AO, Matthews JCF, Politi A, Shadbolt P, et al. Reconfigurable controlled two-qubit operation on a quantum photonic chip. New J Phys. 2011;13:115009.
26. Ibrahim A-BMA, Umarov BA, Wahiddin MRB. Squeezing in the Kerr nonlinear coupler via phase-space representation. Phys Rev A. 2000;61:043804.
27. Hanapi MSM, Ibrahim A-BM, Choudhury PK. On the perturbative approach to analyse entanglement in two-channel Kerr nonlinear coupler. Optik. 2021;243:167420.
28. Hanapi MSM, Ibrahim A-BM, Julius R, Eleuch H. Quantum Kerr nonlinear coupler: analytical versus phase-space method. Can J Phys. 2021;99:832–40.
29. Hanapi MSM, Ibrahim A-BM, Julius R. On the detection of single-mode squeezed states in Kerr nonlinear coupler. J Phys Conf Ser. 2021;2075:012002. IOP Publishing.
30. Julius R, Ibrahim A-BMA, Choudhury PK, Eleuch H. On the nonclassical dynamics of cavity-assisted four-channel nonlinear coupler. Chin Phys B. 2018;27:114206.
31. Julius R, Ibrahim A-BMA, Deni MSM. Quantum state generation in a four-mode Kerr nonlinear directional coupler. Laser Phys. 2014;24:035202.
32. Julius R, Ibrahim A-BM, Choudhury PK, Alias AN, Abd Halim MS. Quantum features of nonlinear coupler with competing nonlinearity. Sci Rep. 2022;12:8245.
33. Julius R, Ibrahim A-BM, Abd-Rahman MK, Choudhury PK. Quantum dynamics of a four-channel Kerr nonlinear directional coupler. Opt Rev. 2018;25:563–70.
34. Julius R, Ibrahim A-BM, Eleuch H, Choudhury PK. Sub-Poissonian photon squeezing and entanglement in optical chain second harmonic generation. J Mod Opt. 2019;66:1129–38.
35. Thapliyal K, Pathak A, Perina J. Linear and nonlinear quantum zeno and anti-zeno effects in a nonlinear optical coupler. Phys Rev A. 2016;93:022107.
36. Korolkova N, Peřina J. Kerr nonlinear coupler with varying linear coupling coefficient. J Mod Opt. 1997;44:1525–34.
37. El-Orany FAA, Perina J, Abdalla MS. Generation of squeezed light in a nonlinear asymmetric directional coupler. J Opt B, Quantum Semiclass Opt. 2001;3:67–75.
38. Drummond PD, Generalised GCW. P-representations in quantum optics. J Phys A, Math Gen. 1980;13:2353.
39. Gilchrist A, Gardiner CW, Drummond PD. Positive P representation: application and validity. Phys Rev A. 1997;55:3014.
40. Sen B, Mandal S. Squeezed states in spontaneous Raman and in stimulated Raman processes. J Mod Opt. 2005;52:1789–807.
41. Mukhopadhyay A. Nonclassical effects in two coupled oscillators at non resonant region. J Phys Commun. 2018;2:055004.
42. Thapliyal K, Pathak A, Sen B, Perina J. Higher order nonclassicalities in a codirectional nonlinear optical coupler: quantum entanglement, squeezing and antibunching. Phys Rev A. 2014;90:013808.
43. Peřina J, Bajer J. Non-classical light in nonlinear symmetric and asymmetric couplers. J Mod Opt. 1995;42:2337–46.

44. Perina J, Perina J Jr. Quantum statistical properties of codirectional and contradirectional nonlinear couplers with phase mismatch. Quantum Semiclassical Opt. 1995;7:863.
45. Perina J, Perina J. Photon statistics of a contradirectional nonlinear coupler. Quantum Semiclassical Opt. 1995;7:849–62.
46. Hanapi MSM, Ibrahim A-BM, Julius R, Choudhury PK. Squeezed light generation in three-channel nonlinear coupler with second-harmonic generation and frequency mismatch. J Phys Conf Ser. 2022;2411:012021. IOP Publishing.
47. Gardiner CW. Handbook of stochastic methods. Berlin: Springer; 1985.
48. Walls DF, Milburn GJ. Quantum optics. Berlin: Springer; 2007.
49. Agarwal GS. Quantum optics. Cambridge: Cambridge University Press; 2012.
50. Snyder AW, Love JD. Optical waveguide theory. London: Chapman & Hall; 1983.
51. Tanzilli S, Martin A, Kaiser F, De Micheli MP, Alibart O, Ostrowsky DB. On the genesis and evolution of integrated quantum optics. Laser Photonics Rev. 2012;6:115–43.
52. Thapliyal K, Pathak A, Sen B, Peřina J. Nonclassical properties of a contradirectional nonlinear optical coupler. Phys Lett A. 2014;378:3431–40.
53. Ariunbold G, Peřina J. Quantum statistics of contradirectional Kerr nonlinear couplers. Opt Commun. 2000;176:149–54.
54. Ding JL, Hou BP, Wang SJ. Squeezing survival and transfer in single and double electromagnetically induced transparency. J Phys B, At Mol Opt Phys. 2010;43:225502.

Publisher's Note